Turk J Phys
30 (2006) , 479 – 492.

Helicity Dependence of the $\vec{\gamma}\vec{N} \to \pi N$ Reaction Channels in the Δ-Resonance Region

E. M. DARWISH and M. A. EL-ZOHRY
Physics Department, Faculty of Science, Sohag University, Sohag 82524, EGYPT
e-mail: eeddarwish@yahoo.com.

Received 10.02.2006

Abstract

Based on a prior effective Lagrangian model on single pion photoproduction from the nucleon, successfully tested in total and differential cross sections, the helicity dependence from the interaction of circularly polarized photons and a longitudinally polarized nucleon target is studied in the energy range from π-threshold through the $\Delta(1232)$-resonance region. The doubly polarized total and differential cross section differences for parallel $\sigma^{3/2}$ and antiparallel $\sigma^{1/2}$ helicity states are predicted and compared with recent experimental data. We show that the results are sensitive to interferences among different contributions to the process and, thus, represent a complementary test of the theoretical model. A quite satisfactory agreement with recent experimental data from the GDH-collaboration is obtained.

Key Words: photoproduction reactions, meson production, polarization phenomena in reactions.

1. Introduction

Since the advent of high duty-factor accelerators, such as MAMI in Mainz and ELSA in Bonn (Germany), JLab in Newport News and LEGS in Brookhaven (USA) or MAX-Lab in Lund (Sweden), the study of single pion production reaction in intermediate energy nuclear physics has been getting more and more attention in recent years (see for example [1–7] and references therein) with respect to the study of hadron structure in the non-perturbative domain of Quantum Chromodynamics (QCD) and therefore the nature of strong interactions. With the developments of these new facilities, it is now possible to obtain accurate data for meson electromagnetic production, including spin-dependent observables.

The difference in the helicity components of total photoabsorption cross section, which determine the Gerasimov-Drell-Hearn (GDH) sum rule, has been measured recently at the Mainz MAMI accelerator, in the energy range from pion threshold up to 800 MeV [8–11]. The study of the helicity structure of pseudoscalar meson photoproduction processes has become of great interest in the field of intermediate energy nuclear physics. The spin asymmetry of the total photoabsorption cross section is of particular interest since it deserves detailed investigations for the various pion production channels. The reason for this is that this asymmetry contains very interesting physics with respect to the hadronic structure of the system.

The main goal of the present paper is to report on a theoretical prediction for the helicity structure of single pion photoproduction channels from the nucleon in the Δ-resonance region. We carry out an analysis of recently published experimental data using double polarization techniques. As stated in [5], such data is very suitable for detailed studies of the production mechanism and properties of excited nucleon resonances.

The work of this paper is organized as follows. In Section 2, we briefly outline the effective Lagrangian model of Schmidt, et al. [12], which we use in our calculation. In Section 3, we present and discuss our results for polarized total and differential cross sections together with a comparison with recent experimental data from the GDH-collaboration [13, 14]. Finally, we conclude and summarize our results in Section 4.

2. The Model

In this section we outline the pion photoproduction operator of Schmidt, et al. [12], which we use in the analysis of this work. The $\mathcal{T}$-operator describing transitions between asymptotically free states is given in terms of the interaction Hamiltonian $\mathcal{H}_{\rm int}$ between all the involved particles as follows [15]:

$$\mathcal{T} = \mathcal{H}_{\rm int} + \mathcal{H}_{\rm int}\frac{1}{E-\mathcal{H}_0+i\epsilon}\mathcal{T}\,, \tag{1}$$

where $\mathcal{H}_0$ is the free Hamiltonian. The on-shell matrix element T_{fi} of (1) is given in terms of the Hamilton operator $\mathcal{H}_{\rm int}$ by

$$T_{fi} = \langle f|\mathcal{T}|i\rangle = \langle f|\mathcal{H}_{\rm int}|i\rangle + \sum_\alpha \langle f|\mathcal{H}_{\rm int}|\alpha\rangle\frac{1}{E-E_\alpha+i\epsilon}T_{\alpha i}\,, \tag{2}$$

where the energy eigenvalues E_α are given by

$$\mathcal{H}_0|\alpha\rangle = E_\alpha|\alpha\rangle\,. \tag{3}$$

Making a one-iteration approximation and keeping terms from the second order we obtain the following expression for the T_{fi}-matrix:

$$T^{(2)}_{fi} = \langle f|\mathcal{H}_{\rm int}|i\rangle + \sum_\alpha \langle f|\mathcal{H}_{\rm int}|\alpha\rangle\frac{1}{E-E_\alpha+i\epsilon}\langle\alpha|\mathcal{H}_{\rm int}|i\rangle\,. \tag{4}$$

The complete Fock space of the system contains N-, πN-, $\pi\pi N$-, $NN\bar{N}$-, $\pi NN\bar{N}$-, Δ-, $\pi\Delta$-, etc., states.

For the process in our case, forms of the initial photon-nucleon state$|i\rangle$ and the final pion-nucleon state $|f\rangle$ are specified by the asymptotical states as

$$|i\rangle = |N,\gamma;\vec{p}_1 s m_s t m_t,\vec{k}\vec{\epsilon}(m_\gamma)\rangle\,, \tag{5}$$
$$|f\rangle = |N',\pi;\vec{p}_2 s' m_{s'} t' m_{t'},\vec{q}\mu\rangle\,, \tag{6}$$

where $\vec{p}_1$, $\vec{p}_2$, $\vec{k}$ and $\vec{q}$ are the momenta of initial and final nucleon, photon and meson, respectively. The isospin projection of the produced pion is given by μ, the polarization vector of the incoming photon by $\vec{\epsilon}$ and m_t and $m_{t'}$ are the isospin projection of the initial and final nucleon, respectively. The states of all particles are covariantly normalized. The individual terms of the T_{fi}-matrix for pion photoproduction on the free nucleon are shown diagrammatically in Figure 1. In the following, we will evaluate the full interaction Hamiltonian of (4) in more details.

The general form of the interaction Hamiltonian of the involved particles, i.e. nucleon, $\Delta(1232)$, pion and photon is described by the operator $\mathcal{H}_{\rm int}$ which is given by

$$\mathcal{H}_{\rm int} = \mathcal{H}_{\rm em} + \mathcal{H}_{\pi N} + \mathcal{H}_{\pi N\Delta}\,, \tag{7}$$

where $\mathcal{H}_{\rm em}$, $\mathcal{H}_{\pi N}$ and $\mathcal{H}_{\pi N\Delta}$ are the Hamiltonians of the electromagnetic interaction, the πN-coupling and the coupling of the $\Delta(1232)$-resonance to the πN system, respectively. In the following, we begin by evaluating the Hamiltonians which describe the interaction between pions, nucleons and photons as well as the contribution of the $\Delta(1232)$-resonance.

2.1. The Electromagnetic Interaction

The electromagnetic interaction $\mathcal{H}_{\rm em}$ contains the coupling of the photon field to the free nucleon, pion and Δ fields

$$\mathcal{H}_{\rm em} = \mathcal{H}_{\gamma N} + \mathcal{H}_{\gamma\pi} + \mathcal{H}_{\gamma\pi N} + \mathcal{H}_{\gamma N\Delta}\,. \tag{8}$$

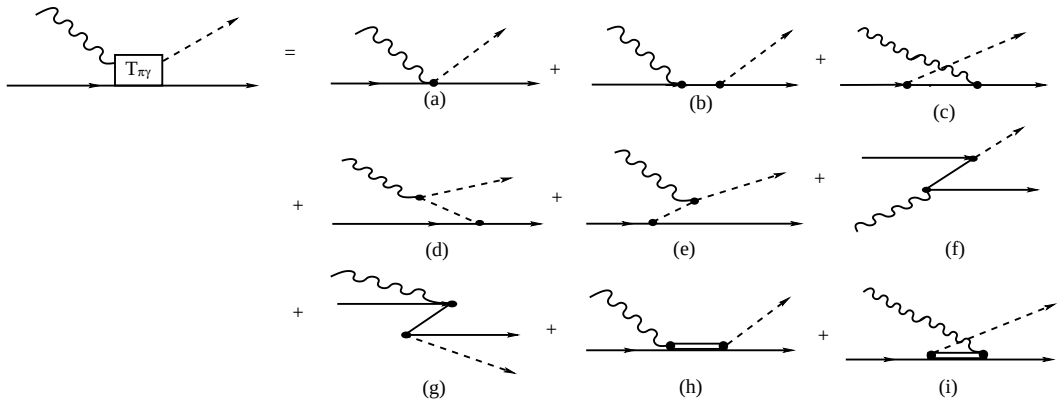

Figure 1. Diagrams for the $\gamma N \to \pi N$ reaction: (a) the Kroll-Rudermann graph, (b) and (c) the two time-ordered contributions to the direct and crossed nucleon pole graph, (d) and (e) the two time-ordered contributions to the pion pole graph, (f) and (g) the Z-graphs and (h) and (i) the $\Delta(1232)$ resonance graphs.

The Hamiltonian corresponding to the absorption of a photon at a nucleon or a pion are given, respectively, by

$$\mathcal{H}_{\gamma N} = -e \int d^3x \bar{\Psi}(\vec{x}) \vec{A}(\vec{x}) \cdot \vec{\gamma} \Psi(\vec{x}) \tag{9}$$

and

$$\mathcal{H}_{\gamma\pi} = \frac{1}{2} \int d^3x \sum_{\mu} (-)^{\mu} ie\mu \vec{A}(\vec{x}) \left[\left(\vec{\nabla} \Phi_{\mu}(\vec{x}) \right) \Phi_{-\mu}(\vec{x}) - \left(\vec{\nabla} \Phi_{-\mu}(\vec{x}) \right) \Phi_{\mu}(\vec{x}) \right], \tag{10}$$

where $\vec{A}(\vec{x})$, $\Psi(\vec{x})$ and $\Phi_{\mu}(\vec{x})$ are the field operators of the photon, nucleon and pion, respectively. $\vec{\gamma}$ represent the Dirac matrices and e denotes the elementary charge.

Using field quantization, the matrix elements are given by

$$\langle N'; \vec{p}_2 m_t' | \mathcal{H}_{\gamma N} | N, \gamma; \vec{p}_1 m_t, \vec{k}\vec{\epsilon} \rangle = -(2\pi)^3 \delta^3(\vec{p}_2 - \vec{p}_1 - \vec{k}) \frac{1}{2M_N} \langle m_t' \mid \left(\hat{e}\,(\vec{p}_2 + \vec{p}_1) + i\,(\hat{e} + \hat{\kappa})\,\vec{\sigma} \times \vec{k} \right) \cdot \vec{\epsilon} \mid m_t \rangle \tag{11}$$

and

$$\langle \pi; \vec{q}'\mu' | \mathcal{H}_{\gamma\pi} | \pi, \gamma; \vec{q}\mu, \vec{k}\vec{\epsilon} \rangle = -(2\pi)^3 \delta^3(\vec{q}' - \vec{q} - \vec{k}) \delta_{\mu\mu'} e\mu (\vec{q} + \vec{q}') \cdot \vec{\epsilon}, \tag{12}$$

where M_N is the nucleon mass and $\vec{\sigma}$ are the Pauli spin matrices. $\hat{e}$ and $\hat{\kappa}$ denote nucleon charge and anomalous part of the nucleon magnetic moment, respectively.

In addition to the matrix elements of (11) and (12), the following matrix element of $\mathcal{H}_{\pi\gamma}$ between a state of two-pion and one photon is considered

$$\langle \pi, \pi'; \vec{q}\mu, \vec{q}'\mu' | \mathcal{H}_{\pi\gamma} | \gamma; \vec{k}\vec{\epsilon} \rangle = -(2\pi)^3 \delta^3(\vec{q}' + \vec{q} - \vec{k}) \delta_{-\mu\mu'} e\mu (\vec{q} + \vec{q}') \cdot \vec{\epsilon}. \tag{13}$$

This matrix element will be used later in the construction of the amplitude of diagrams (d) and (e) in Figure 1. The pionic current terms, which are given in (12) and (13), contribute only to the photoproduction of charged pions.

The $\gamma\pi N$ Hamiltonian is given by

$$\mathcal{H}_{\gamma\pi N} = \frac{i f_{\pi N}}{m_{\pi}} \sum_{\mu=\pm 1,0} \int d^3x \bar{\Psi}(\vec{x}) \vec{\gamma} \cdot \vec{A}(\vec{x}) \gamma_5 \left[\hat{e}, \tau_{\mu}^{+} \right] \Psi(\vec{x}) \Phi_{\mu}(\vec{x}), \tag{14}$$

where m_π is the pion mass and $\vec{\tau}$ represent the isospin matrices. We used the πN coupling constant $\frac{f^2_{\pi N}}{4\pi} = 0.0735$ which is given in [16] by fitting the πN scattering data. The $\gamma\pi N$ Hamiltonian is linear in photon and pion fields. This leads to a vertex, in which both photon and pion couple to the nucleon. The matrix element of $\mathcal{H}_{\gamma\pi N}$ is given by

$$\langle N', \pi; \vec{p}_2 m'_t, \vec{q}\mu | \mathcal{H}_{\gamma\pi N} | N, \gamma; \vec{p}_1 m_t, \vec{k}\vec{\epsilon}\rangle \;=\; (2\pi)^3 \delta^3(\vec{p}_2 + \vec{q} - \vec{p}_1 - \vec{k}) \; \frac{i f_{\pi N}}{m_\pi} \langle m'_t \mid \vec{\sigma}\cdot\vec{\epsilon}\left[\hat{e}, \tau^+_\mu\right] \mid m_t\rangle \,. \quad (15)$$

This matrix element contributes only to the photoproduction of charged pions.

Now, we evaluate the fourth term in (8). In the description of the $\gamma N\Delta$-vertex one has to take into account the magnetic dipole $M1$ and a possible electric quadrupole $E2$ excitation of the Δ resonance

$$\mathcal{H}_{\gamma N\Delta} \;=\; \mathcal{H}^{M1}_{\gamma N\Delta} + \mathcal{H}^{E2}_{\gamma N\Delta} \,. \quad (16)$$

Since the strength of the electric quadrupole excitation $E2$ is much smaller than the magnetic dipole one (see for example [17, 18]) we will neglect it in this work. Following Wilhelm and Arenhövel [17] and Weber and Arenhövel [19], the $\gamma N\Delta$ vertex reads

$$\mathcal{H}_{\gamma N\Delta} \;=\; \frac{ieG^{M1}_{\Delta N}(W_{\pi N})}{2M_N} \; \vec{\sigma}_{\Delta N}\cdot(\vec{k}\times\vec{\epsilon}) \; \tau_{\Delta N,0} \,. \quad (17)$$

Here, $W_{\pi N}$ denotes the invariant mass of the πN-subsystem and it is given by

$$W_{\pi N} \;=\; E_N(q_{\text{c.m.}}) + \omega_\pi(q_{\text{c.m.}}) \,, \quad (18)$$

where $E_N = \sqrt{M_N^2 + q^2_{\text{c.m.}}}$ and $\omega_\pi = \sqrt{m_\pi^2 + q^2_{\text{c.m.}}}$ with the center of mass pion momentum being $q_{\text{c.m.}}$. The transition spin (isospin) operator $\vec{\sigma}_{N\Delta} = \vec{\sigma}^\dagger_{\Delta N}$ ($\vec{\tau}_{N\Delta} = \vec{\tau}^\dagger_{\Delta N}$) is normalized as

$$\langle \frac{3}{2} \,||\, \sigma_{\Delta N}(\tau_{\Delta N}) \,||\, \frac{1}{2}\rangle \;=\; -\langle \frac{1}{2} \,||\, \sigma_{N\Delta}(\tau_{N\Delta}) \,||\, \frac{3}{2}\rangle \;=\; 2 \,. \quad (19)$$

The energy dependent and complex coupling $G^{M1}_{\Delta N}(W_{\pi N})$ is given as in [17] by

$$G^{M1}_{\Delta N}(W_{\pi N}) = \begin{cases} \mu^{M1}(W_{\pi N}) e^{i\Phi^{M1}(W_{\pi N})} & \text{for} \quad W_{\pi N} > m_\pi + M_N \\ 0 & \text{else} \end{cases} \,, \quad (20)$$

where $\mu^{M1}(W_{\pi N})$ is given by

$$\mu^{M1}(W_{\pi N}) = \mu_0 + \mu_2 \left(\frac{q_\Delta}{m_\pi}\right)^2 + \mu_4 \left(\frac{q_\Delta}{m_\pi}\right)^4 \quad (21)$$

and the phase $\Phi^{M1}(W_{\pi N})$ by [20]

$$\Phi^{M1}(W_{\pi N}) = \frac{q^3_\Delta}{a_1 + a_2 q^2_\Delta} \,. \quad (22)$$

q_Δ is the on-shell pion momentum in the πN center of mass frame on the top of the resonance, i.e., when the invariant mass $W_{\pi N}$ of the πN state equals the mass of the Δ resonance

$$W_{\pi N} = \omega_\pi(q_\Delta) + E_N(q_\Delta) \;=\; M_\Delta \,. \quad (23)$$

It is given by

$$q_\Delta = \sqrt{\frac{\left(W^2_{\pi N} - m^2_\pi - M^2_N\right)^2 - 4m^2_\pi M^2_N}{4W^2_{\pi N}}} \,. \quad (24)$$

The free parameters $\mu_0 = 4.16$, $\mu_2 = 0.542$, $\mu_4 = -0.0757$, $a_1 = 0.185$ fm^{-3} and $a_2 = 4.94$ fm^{-1} are fitted to the experimental data for the $M^{3/2}_{1+}$-multipole of pion photoproduction [21, 17], i.e. the parameters have chosen consistent with the Born terms in the $M1$ channel. Due to the use of a constant Δ mass in the Δ propagator we had to increase $G^{M1}_{\Delta N}$ from [17] by a factor of 1.15 to fit the experimental $M^{3/2}_{1+}$ multipole.

2.2. The πN Interaction

The πN interaction operator in pseudovector coupling is given by

$$\mathcal{H}_{\pi N} = -\frac{f_{\pi N}}{m_\pi}\int d^3x\bar{\Psi}(\vec{x})\vec{\gamma}\cdot\gamma_5\vec{\tau}\cdot\Psi(\vec{x})\vec{\nabla}\vec{\Phi}(\vec{x})\,. \tag{25}$$

This operator is linear in the pion field operator $\vec{\Phi}(\vec{x})$. Therefore, only one pion can be produced or absorbed at the πN-vertex. Thus, only two possible diagrams contribute. The evaluation of these two graphs yields the matrix elements

$$\langle N',\pi;\vec{p}_2 m_t',\vec{q}\mu|\mathcal{H}_{\pi N}|N;\vec{p}_1 m_t\rangle = -(2\pi)^3\delta^3(\vec{p}_2+\vec{q}-\vec{p}_1)\,\frac{if_{\pi N}}{m_\pi}\,\langle m_t' \mid \vec{q}\cdot\vec{\sigma}\tau_\mu^+ \mid m_t\rangle \tag{26}$$

for the emission of a pion and

$$\begin{aligned}\langle N',\pi;\vec{p}_2 m_t',\vec{q}\mu|\mathcal{H}_{\pi N}|N,\pi_1,\pi_2;\vec{p}_1 m_t,\vec{q}_1\mu_1,\vec{q}_2\mu_2\rangle &= -(2\pi)^6\,\frac{2if_{\pi N}}{m_\pi}\\ \times\ \big[\delta^3(\vec{p}_2-\vec{q}_1-\vec{p}_1)\delta^3(\vec{q}-\vec{q}_2)\delta_{\mu\mu_2}\omega_{\vec{q}_2}(-)^{\mu_1}\langle m_t' \mid \tau_{\mu_1}\vec{q}_1\cdot\vec{\sigma} \mid m_t\rangle\\ +\,\delta^3(\vec{p}_2-\vec{q}_2-\vec{p}_1)\delta^3(\vec{q}-\vec{q}_1)\delta_{\mu\mu_1}\omega_{\vec{q}_1}(-)^{\mu_2}\langle m_t' \mid \tau_{\mu_2}\vec{q}_2\cdot\vec{\sigma} \mid m_t\rangle\big]\end{aligned} \tag{27}$$

for the absorption of a pion, where $\omega_{\vec{q}_i}=\sqrt{m_\pi^2+q_i^2}$ is the energy of the pion with momentum $\vec{q}_i$.

2.3. The $\pi N\Delta$-Vertex

Here, we will evaluate the $\pi N\Delta$-vertex which contribute to the amplitude of the Δ-resonance. For the $\pi N\Delta$-vertex we use [17, 19]

$$\mathcal{H}_{\pi N\Delta} = -\frac{i}{m_\pi}F_\Delta(q^2)\,(-)^\mu\,\vec{\tau}_{N\Delta,-\mu}\,\vec{\sigma}_{N\Delta}\cdot\vec{q}. \tag{28}$$

We have introduced a hadronic monopole form factor:

$$F_\Delta(q^2)=f_{\pi N\Delta}\frac{\Lambda_\Delta^2+q_\Delta^2}{\Lambda_\Delta^2+q^2}\,. \tag{29}$$

The coupling constant $\frac{f^2_{\pi N\Delta}}{4\pi}=1.393$ and the cutoff $\Lambda_\Delta=315$ MeV are fixed in [17, 22] to fit the πN scattering phase shift in the P_{33} channel and are also used in this work.

Using the Hamilton operator (7) and taking into account all possible intermediate states $|\alpha\rangle$ in (4), one can calculate the on-shell T_{fi}-matrix for pion photoproduction on the nucleon by constructing the lowest order diagrams as shown in Figure 1. The quality of the model can be judged by a comparison with the MAID analysis [23], the Mainz dispersion analysis [24] and the VPI analysis from the SAID program [21] as shown in Figure 1 of [25], and quite a good agreement was achieved.

3. Results and Discussion

In this section, we will classify our discussion into two classes. In the first class, we offer the results for polarized total cross sections for circularly polarized photons on a longitudinally polarized nucleon target with spin parallel $\sigma^{3/2}$ and spin antiparallel $\sigma^{1/2}$ to the photon spin for the different pion photoproduction channels in comparison with the available experimental data. Results for the helicity difference $\sigma^{3/2}-\sigma^{1/2}$, i.e., the spin asymmetry of the nucleon, will be also presented and discussed in this class. In the second class, we present and discuss the results for polarized differential cross section difference $(d\sigma/d\Omega)^{3/2}-(d\sigma/d\Omega)^{1/2}$ for the four isospin channels. In our comparison with experiment, we concentrate our discussion on π^0- and π^+-production on the proton since data for π^0- and π^--production on the neutron are not available with respect to the absent of any free neutron targets.

3.1. Polarized Total Cross Section

We start the discussion with the presentation of our results in Figures 2 through 5, of cross sections for circularly polarized photons on a longitudinally polarized nucleon target with spin parallel $\sigma^{3/2}$ (upper parts: left), spin antiparallel $\sigma^{1/2}$ (upper parts: right) to the photon spin and the spin asymmetry $\sigma^{3/2}-\sigma^{1/2}$ (lower parts). The solid curves show the results of the full calculation, i.e., when both the Born terms and the contribution from the Δ-resonance are taken into account. The dashed curves denote the results when only the contribution from the Born terms is considered. The dash-dotted curves display the results when the contribution from the Δ-resonance is neglected and the anomalous magnetic moment of the nucleon is vanishing, i.e., $T_{fi}^{\Delta}=0$ and $\kappa_N=0$. The helicity dependent total cross sections give valuable information on the nucleon spin structure and allow the determination of the dominant contribution to the GDH integral.

In general, one sees qualitatively a different behaviour for polarized total cross sections in case of the charged (Figures 2 and 4) and the neutral (Figures 3 and 5) pion production channels. In the case of π^+-production on the proton (Figure 2), one can see that $\sigma^{3/2}$, $\sigma^{1/2}$ and their difference $\sigma^{3/2}-\sigma^{1/2}$ have a peak at energy in the region of the $\Delta(1232)$-resonance. In case of the π^0-production on the proton (Figure 3), one notes that $\sigma^{3/2}$, $\sigma^{1/2}$ and their difference $\sigma^{3/2}-\sigma^{1/2}$ have also a peak at energy in the region of the

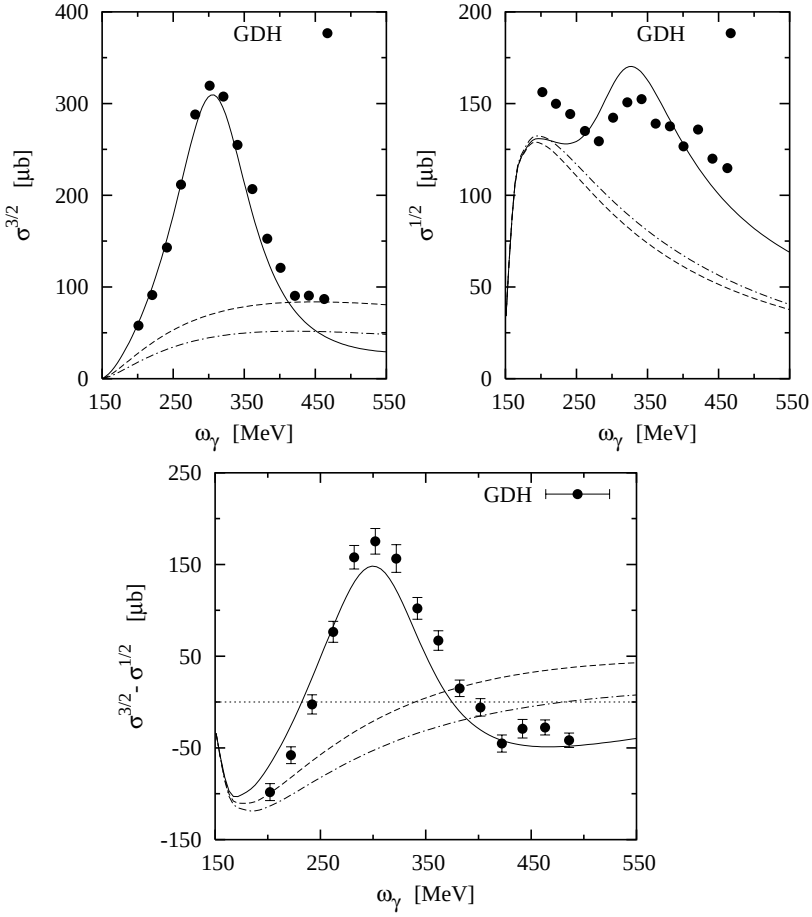

Figure 2. Total photoabsorption cross sections for circularly polarized photons on a longitudinally polarized nucleon target with spin parallel $\sigma^{3/2}$ (upper part: left) and antiparallel $\sigma^{1/2}$ (upper part: right) to the photon spin for the reaction $\vec{\gamma}\vec{p}\to n\pi^+$ as a function of photon lab-energy. Lower part shows the difference of the total cross sections. The solid (dashed) curve shows the results using the Born terms with (without) the Δ-resonance contribution. The dash-dotted curve shows the results of Born terms when $\kappa_N=0$. The experimental data are from the GDH-collaboration [13, 14].

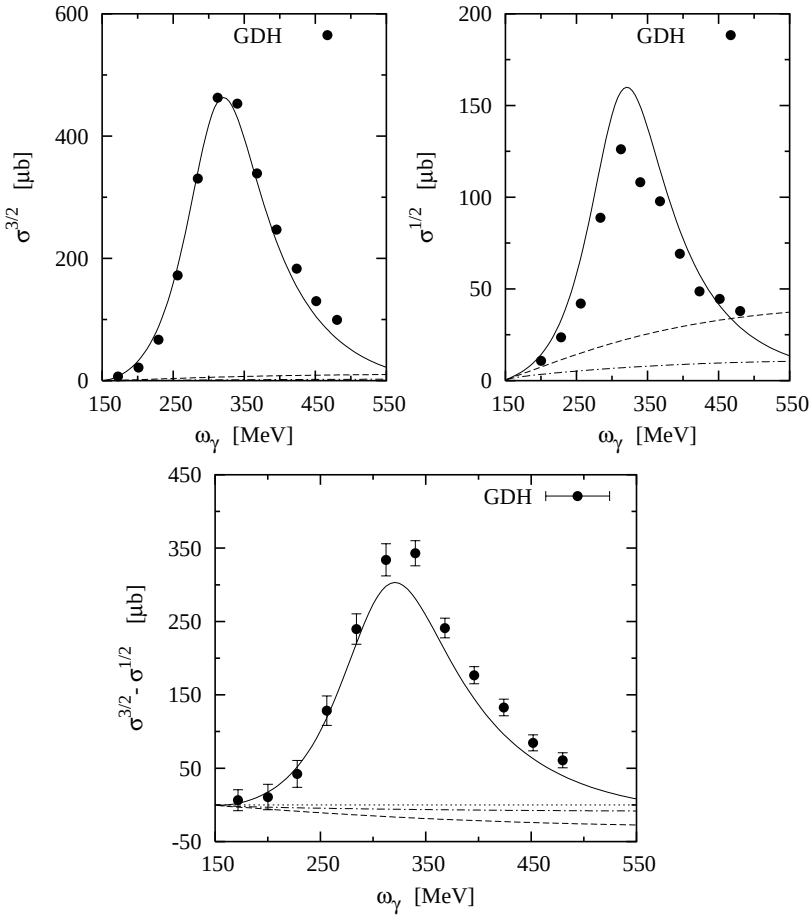

Figure 3. Same as in Figure 2, but for the $\vec{\gamma}\vec{p} \to p\pi^0$ channel.

$\Delta(1232)$-resonance, which comes mainly from the contribution of the Δ-excitation. Qualitatively, one notes that $\sigma^{3/2}$ and $\sigma^{1/2}$ have a similar behaviour in the case of π^0- and π^+-production on the proton.

It is also clear from the dashed curves in Figures 2 through 5 that the contribution from Born terms is small, in particular when both the photon and the nucleon have parallel spins. Obviously, from the GDH sum rule relation,

$$\frac{\pi e^2 \kappa_N^2}{2M_N^2} = \int_{\omega_{\rm thr}}^{\infty} \frac{\sigma^{3/2}(\omega_\gamma) - \sigma^{1/2}(\omega_\gamma)}{\omega_\gamma} d\omega_\gamma, \tag{30}$$

that for $\kappa_N \neq 0$, the particle possesses an internal structure. However, the opposite is not in general true. A particle having a vanishing or very small κ_N need not be point-like or nearly point-like. When the anomalous magnetic moment of the nucleon goes to zero, one observes that $\sigma^{3/2}$ is smaller than $\sigma^{1/2}$ and therefore the spin asymmetry $\sigma^{3/2} - \sigma^{1/2}$ has negative values. In contrast to the neutral pion channels, we see that the spin asymmetry $\sigma^{3/2} - \sigma^{1/2}$ for charged pion production channels starts with negative values. These negative values come from higher values in $\sigma^{1/2}$.

In comparison with the most recent experimental data from the GDH-collaboration [13, 14], it is interesting to note that $\sigma^{3/2}$ has good agreement, but small discrepancies are found in the case of $\sigma^{1/2}$, especially in the peak region. The agreement of our results for the spin asymmetry $\sigma^{3/2} - \sigma^{1/2}$ with the GDH data [13, 14] is good. Only at energies in the Δ-region a small underestimation is found which result from an overestimation in $\sigma^{1/2}$.

Figures 4 and 5 show the results for total photoabsorption cross sections of π^-- and π^0-production on the neutron, respectively. Because the neutron has a short lifetime, free neutron targets are not available for

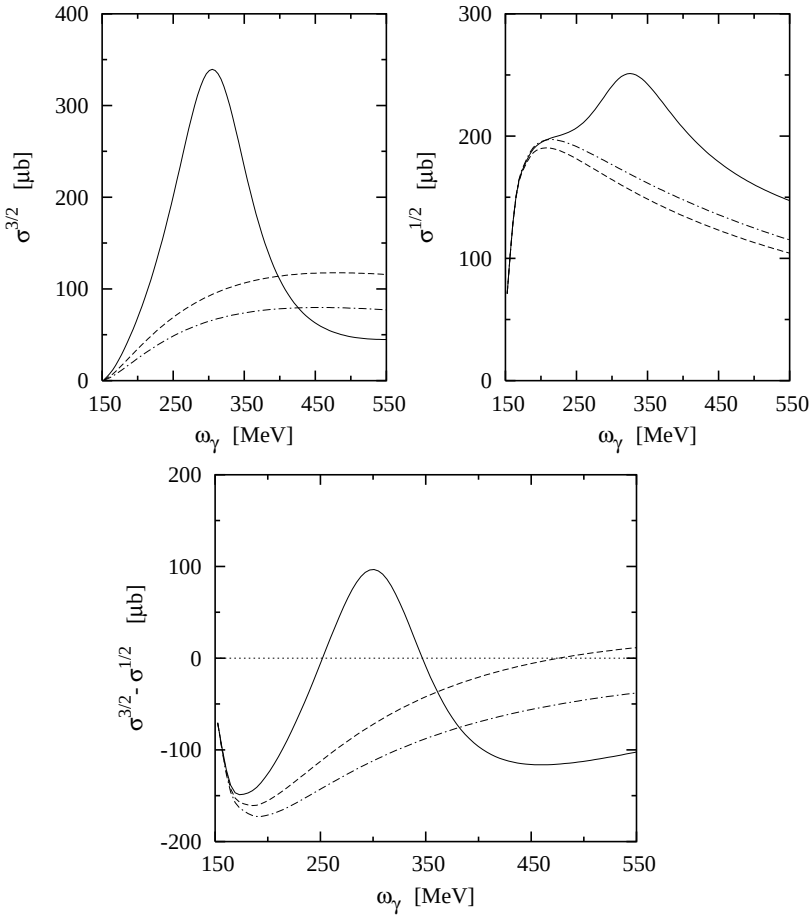

Figure 4. Same as in Figure 2, but for the $\vec{\gamma}\vec{n} \to p\pi^-$ channel.

the study of the neutron channels, and thus one shows no comparison of our predictions with experimental data in Figures 4 and 5. In case of the π^0-production on the neutron (Figure 5), one notes that $\sigma^{3/2}$, $\sigma^{1/2}$ and their difference have a peak at energy in the region of the $\Delta(1232)$-resonance. It is also clear from the dashed curves that the contribution from Born terms is negligible, in particular in the case of $\sigma^{3/2}$. When the anomalous magnetic moment of the nucleon goes to zero, one observes that $\sigma^{3/2}$ and $\sigma^{1/2}$ and therefore the spin asymmetry $\sigma^{3/2} - \sigma^{1/2}$ vanish.

In the case of π^+- and π^--production (see Figures 2 and 4, respectively), we see that in the energy region close to threshold the polarized total cross section $\sigma^{1/2}$ is much greater than $\sigma^{3/2}$. Therefore, the helicity difference $\sigma^{3/2} - \sigma^{1/2}$ (see the lower parts in Figures 2 and 4) becomes negative and changes much more strongly than the unpolarized total cross sections (compare with the results of unpolarized total cross sections presented in [25]). The reason for that stems from the fact that, in the energy region close to threshold, the pion production reaction is dominated by the s-wave (intermediate states with spin $\frac{1}{2}$). These states contribute only to the polarized cross section $\sigma^{1/2}$. On the contrary, in the energy region of the $\Delta(1232)$-resonance, it is clear from the upper part of Figures 2 and 4 that the polarized total cross section $\sigma^{1/2}$ is much smaller than $\sigma^{3/2}$ since the transition in this case is essentially $M1$. Therefore, the helicity difference $\sigma^{3/2} - \sigma^{1/2}$ is found to be large and positive in this case. The reason for that comes from the fact that in the energy region of the $\Delta(1232)$-resonance (intermediate state with spin $\frac{3}{2}$) both helicity cross sections contribute.

We would like to close with a short discussion on the dash-dotted curves in Figures 2 through 5 which indicate the results using a very simple model for pion photoproduction on the nucleon. In this model we put

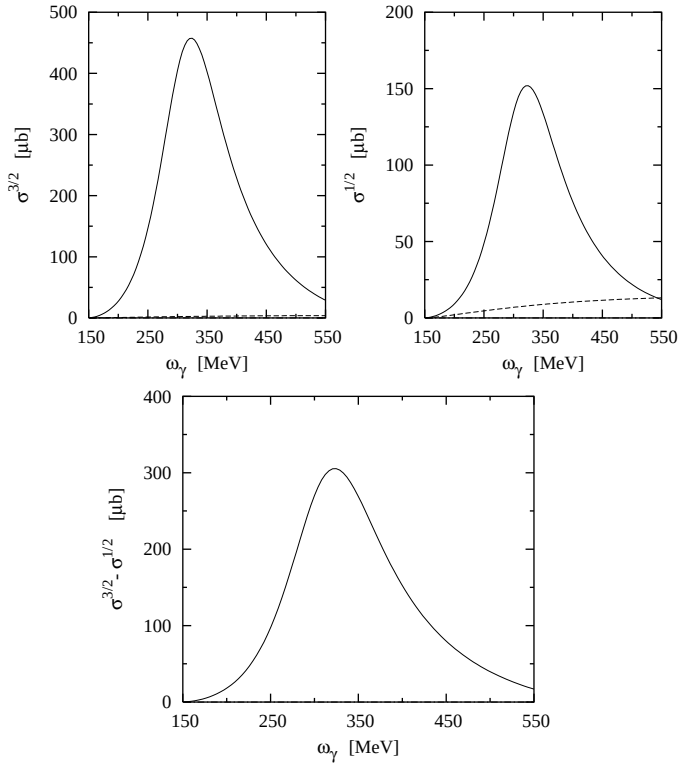

Figure 5. Same as in Figure 2, but for the $\vec{\gamma}\vec{n} \to n\pi^0$ channel.

a zero value for the anomalous magnetic moment of the nucleon, i.e., $\kappa_N = 0$, and neglect the contribution from the Δ-resonance, i.e., $T_{fi}^{\Delta} = 0$. As a result one sees that the production of the π^0-meson is suppressed very strongly. In the case of π^0-production on the neutron, it disappears completely. The reason for that stems from the fact that the neutron is a neutral particle and therefore the photon can attack with the production of the π^0-meson only on the anomalous magnetic moment, which was switched off in this very simple model. This suppression of the cross section does not arise however with the charged pions, the amount of $\sigma^{3/2}$, $\sigma^{1/2}$ and hence $\sigma^{3/2} - \sigma^{1/2}$ becomes larger still.

3.2. Polarized Differential Cross Section

Next, we consider the polarized differential cross section difference $d(\sigma^{3/2} - \sigma^{1/2})/d\Omega$, as shown in Figures 6 through 9, as a function of the emission pion angle θ_π in the c.m. system at nine different values of photon energies in the lab-frame. As in the case of polarized total cross sections, the solid curves show the results when both Born terms and the contribution from the Δ-resonance are taken into account, the dashed curves denote the results when only the contribution from Born terms is considered and the dash-dotted curves display the results when the contribution from the Δ-resonance is neglected and the anomalous magnetic moment of the nucleon is vanishing. One notes that the helicity difference $d(\sigma^{3/2} - \sigma^{1/2})/d\Omega$ has a peak at $\theta_\pi \simeq 90^\circ$ for all energies. It is obvious from the dashed curves that the contribution from Born terms is approximately negligible since a very strong reduction in the helicity difference appears. As in the case of polarized total cross sections, the results when $T_{fi}^{\Delta} = 0$ and $\kappa_N = 0$ vanish in the case of neutral pion channels and therefore the dash-dotted curves are not seen. At extreme forward and backward pion angles, it is very obvious that the helicity difference is vanishing.

In the case of charged pion production channels (Figures 6 and 8), one sees that the situation is similar to the case of polarized total cross section. The dashed curves in these two figures demonstrate the impor-

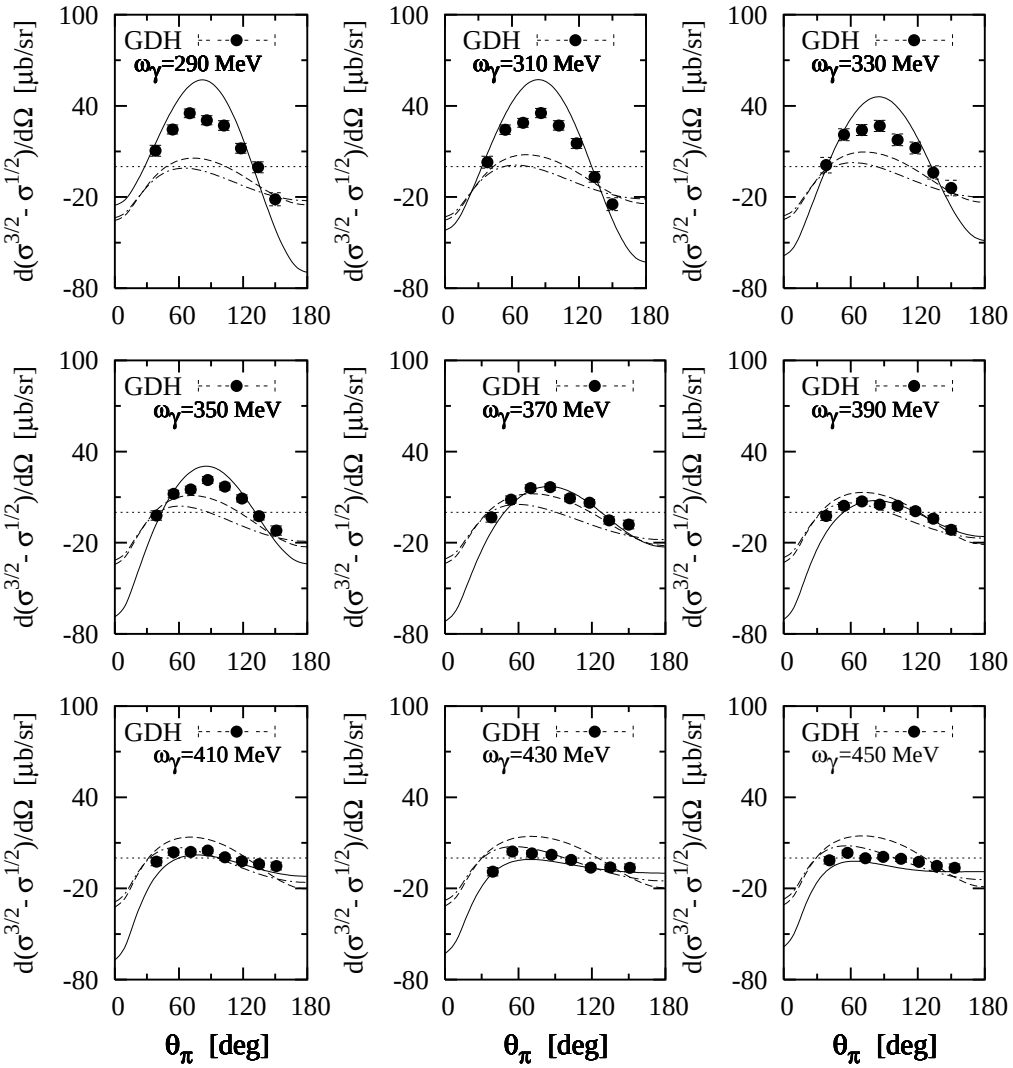

Figure 6. The helicity difference $d(\sigma^{3/2} - \sigma^{1/2})/d\Omega$ of polarized differential cross sections for the reaction $\vec{\gamma}\vec{p} \to n\pi^+$ as a function of pion angle in the c.m. frame at nine different values of photon lab-energy. The experimental data are from the GDH-collaboration [13, 14]. Notation of curves as in Figure 2.

tance of Born terms. At extreme forward and backward pion angles, it is very obvious that the difference $d(\sigma^{3/2} - \sigma^{1/2})/d\Omega$ has negative values which come mainly from higher positive values in $(d\sigma/d\Omega)^{1/2}$. For π^0-production on the proton (Figure 7) and neutron (Figure 9), one observes small negative values at extreme backward angles which stem from small positive values in $(d\sigma/d\Omega)^{3/2}$.

Figure 6 displays that the results for polarized differential cross section difference $d(\sigma^{3/2} - \sigma^{1/2})/d\Omega$ for the reaction $\vec{\gamma}\vec{p} \to n\pi^+$ are in good agreement with the recent experimental data from [13, 14], in particular at high energies. A small overestimation at small energies, especially in the peak region, is found. Figure 7 shows the results for the helicity difference of the reaction $\vec{\gamma}\vec{p} \to p\pi^0$ in comparison with the data from [13, 14]. One readily sees that discrepancies are obtained in this case, in particular at small energies. At energies above the region of the Δ-resonance, a very small deviation is obtained. An experimental check of these predictions at extreme forward and backward pion angles is needed. Furthermore, an independent evaluation in the framework of effective field theory would be very interesting.

The calculations we have predicted in the present work are just an example of the type of studies that one can make, in the same way that other energies, angles or kinematical cuts can be implemented, and it serves

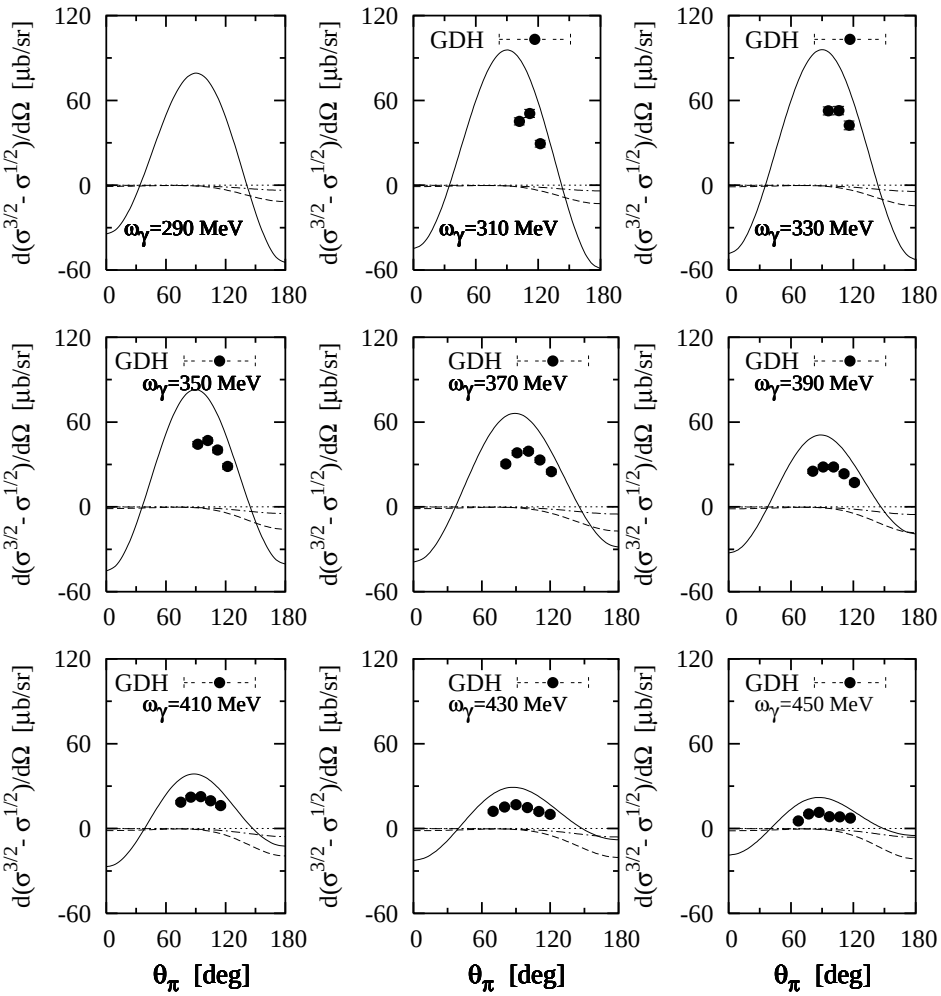

Figure 7. Same as in Figure 6, but for the $\vec{\gamma}\vec{p} \to p\pi^0$ channel.

as an example of the strong dependence on interferences that is obtained from such kinds of polarization experiments.

4. Summary

In this paper, we have presented theoretical predictions of the helicity dependence for the interaction of circularly polarized photons with longitudinally polarized nucleon target, $\vec{\gamma}\vec{N} \to \pi N$. We have used a well tested theoretical model successfully applied in the evaluation of several unpolarized observables. The helicity dependent total and differential cross sections give valuable information on the nucleon spin structure and allow the determination of the dominant contribution to the GDH integral.

The main conclusions of this work are summarized as follows. In the case of total photoabsorption cross sections for circularly polarized photon on a longitudinally polarized nucleon target with spin parallel $\sigma^{3/2}$, spin antiparallel $\sigma^{1/2}$ to the photon spin and the spin asymmetry $\sigma^{3/2} - \sigma^{1/2}$, we obtained qualitatively a similar behaviour for the polarized total cross sections in the case of charged pion production channels, whereas a totally different one is seen in the case of neutral channels. The threshold region is dominated by the s-wave pion production that can only contribute to the cross section $\sigma^{1/2}$. In the $\Delta(1232)$-resonance region, we found that the helicity difference $\sigma^{3/2} - \sigma^{1/2}$ became large and positive. In comparison with

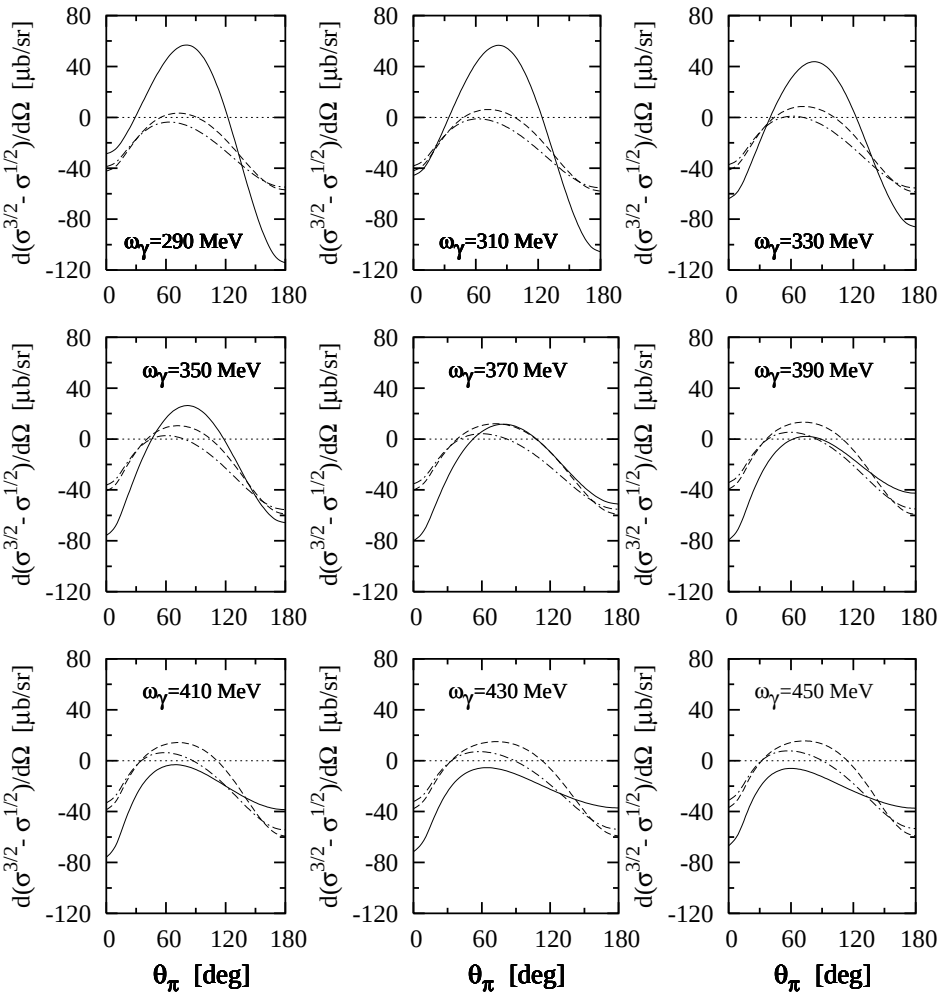

Figure 8. Same as in Figure 6, but for the $\vec{\gamma}\vec{n} \to p\pi^-$ channel.

experiment, we found that the $\sigma^{3/2}$ curve has a good agreement with experiment; but in the case of $\sigma^{1/2}$ curve, especially in the peak region, small discrepancies are found. The agreement of the results for spin asymmetry $\sigma^{3/2} - \sigma^{1/2}$ is found to be good. Only at energies in the Δ-region, a small underestimation is found which stems from an overestimation in $\sigma^{1/2}$.

With respect to the results for differential photoabsorption cross section difference $d(\sigma^{3/2} - \sigma^{1/2})/d\Omega$, we observed a peak when $\theta_\pi \simeq 90^\circ$ in the case of charged and neutral pion production channels. When the photon energy was increasing, the top of this peak changed from higher to smaller values. Small negative values for the helicity difference appear only at extreme backward angles, which came from small positive values in $(d\sigma/d\Omega)^{3/2}$. At extreme forward and backward pion angles, we found that the helicity difference $d(\sigma^{3/2} - \sigma^{1/2})/d\Omega$ had negative values which came from positive values in $(d\sigma/d\Omega)^{1/2}$. In comparison with experimental data, discrepancies are obtained in the case of π^0-production on the proton, especially at small energies. At energies above the region of the Δ-resonance, a very small deviation has been obtained. For π^+-production on the proton, we found that the results were in good agreement with experiment. Small discrepancies were found only at small energies, especially in the peak region.

This work could be continued by further refinement of the pion production operator. Modifying this operator above the two pion threshold may improve our results for the spin asymmetry and the corresponding GDH sum rule for the nucleon [26]. This may also result in a better agreement between experimental data and theoretical predictions.

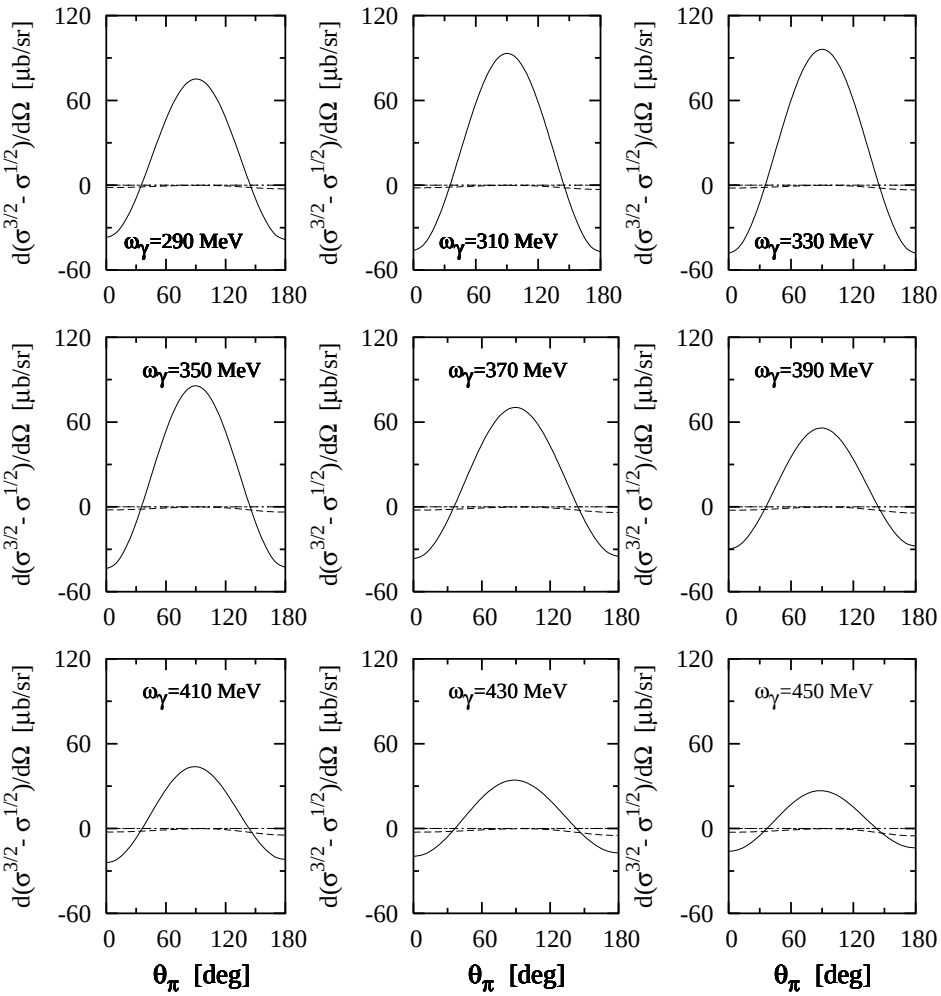

Figure 9. Same as in Figure 6, but for the $\vec{\gamma}\vec{n} \to n\pi^0$ channel.

Acknowledgments

We would like to thank the members of the GDH-collaboration at Mainz, Germany for providing us with their experimental data.

References

[1] Proceedings of the 2nd Int. Symposium on the *Gerasimov-Drell-Hearn 2002 Sum Rule and the Spin Structure of the Nucleon*, Genova, Italy, 3-6 July, 2002, ed. by M. Anghinolfi, M. Battaglieri, R. De Vita, (World Scientific, Singapore, 2003).

[2] Proceedings of the NSTAR2002 Workshop on the *Physics of Excited Nucleons*, Pittsburgh, Pennsylvania, USA, 9-12 October, 2002, ed. by S. A. Dytman and E. S. Swanson (World Scientific, Singapore, 2003).

[3] Proceedings of the NSTAR2004 Workshop on the *Physics of Excited Nucleons*, Grenoble, France, 24-27 March, 2004.

[4] Proceedings of the 10^{th} International Symposium on *Meson-Nucleon Physics and the Structure of the Nucleon (MENU04)*, Beijing, China, August 29–Sept. 4, 2004.

[5] B. Krusche, S. Schadmand, *Prog. Part. Nucl. Phys.,* **51**, (2003), 399.

[6] V. Burkert, T-S.H. Lee, *Int. J. Mod. Phys.,* **E13**, (2004), 1035.

[7] D. Drechsel, L. Tiator, *Ann. Rev. Nucl. Part. Sci.,* **54**, (2004), 69.

[8] J. Ahrens, et al., *Phys. Rev. Lett.,* **84**, (2000), 5950.

[9] J. Ahrens, et al., *Phys. Rev. Lett.,* **87**, (2001), 022003.

[10] J. Ahrens, et al., *Phys. Rev. Lett.,* **88**, (2002), 232002.

[11] J. Ahrens, et al., *Phys. Lett.,* **B551**, (2003), 49.

[12] R. Schmidt, H. Arenhövel, P. Wilhelm, *Z. Phys.,* **A355**, (1996), 421.

[13] J. Ahrens, et al., *Eur. Phys. J.,* **A21**, (2004), 323.

[14] I. Preobrajenski, PhD Thesis, Institut für Kernphysik, Johannes Gutenberg-Universität, Mainz, 2001.

[15] C. J. Joachain, *Quantum Collision Theory*, North-Holland Publishing Company, Amsterdam, New York, Oxford, 1979.

[16] R. A. Arndt, Z. Li, L. D. Roper, R. L. Workman, *Phys. Rev. Lett.,* **65**, (1990), 157.

[17] P. Wilhelm, H. Arenhövel, *Nucl. Phys.,* **A593**, (1995), 435.

[18] R. M. Davidson, N. C. Mukhopadhyay, R. S. Wittman, *Phys. Rev.,* **D43**, (1991), 71.

[19] H. J. Weber, H. Arenhövel, *Phys. Rep.,* **36**, (1978), 277.

[20] J. H. Koch, N. Ohtsuka, E. J. Moniz, *Ann. Phys.,* **154**, (1984), 99.

[21] R. A. Arndt, et al., *The Scattering Analysis Interactive Dial-In Program (SAID)*, data available via telnet to VTINTE.PHYS.VT.EDU, Virginia Polytechnic Institute, Blacksburg, Virginia. For further references see, for example, R. A. Arndt, I. I. Strakovsky, R. L. Workman, *Phys. Rev.,* **C53**, (1996), 430; R. A. Arndt, R. L. Workman, Z. Li, L. D. Roper, *Phys. Rev.,* **C42**, (1990), 1853.

[22] H. Poepping, P. U. Sauer, X.-Z. Zhang, *Nucl. Phys.,* **A474**, (1987), 557.

[23] D. Drechsel, O. Hanstein, S. Kamalov, L. Tiator, *Nucl. Phys.,* **A645**, (1999), 145; *MAID Program*, Institut für Kernphysik, Johannes Gutenberg-Universität, Mainz, Germany, http://www.kph.uni-mainz.de/de/MAID/.

[24] O. Hanstein, D. Drechsel, L. Tiator, *Nucl. Phys.,* **A632**, (1998), 561.

[25] E. M. Darwish, H. Arenhövel, M. Schwamb, *Eur. Phys. J.,* **A16**, (2003), 111.

[26] E. M. Darwish, M. A. El-Zohry, *Act. Phys. Pol.,* **B37**, (2006), 463.